CONFINEMENT EFFECTIVENESS OF LATERAL REINFORCEMENT ARRANGEMENTS IN CORE CONCRETE

(Reprinted from Journal of Materials, Concrete Structures and Pavements, No. 520, V-28, 1995)

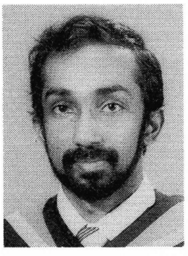
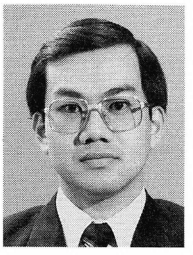
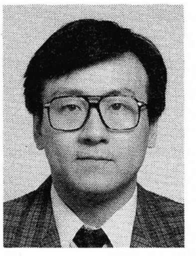

Tirath M. PALLEWATTA Paulus IRAWAN Koichi MAEKAWA

The behavior of concrete confined by lateral reinforcement is evaluated using an experimental approach. The primary objectives of the experimental study are to mechanically define the confinement effect of lateral reinforcement layouts and to obtain reliable data for verification of a non-linear, three-dimensional concrete constitutive law under the non-uniform stress fields produced in the confined concrete cores of column members. A further aim is to identify the influence of detailing parameters on the confinement phenomena for the purpose of developing and examining a behavior-oriented macro-model. A three-dimensional elasto-plastic and continuum fracture model for concrete, which was originally developed in relation to uniform stress fields, is verified at the structural member level, which the stress fields are not uniform. Idealized square concrete cores confined only by closed square lateral steel ties are adopted in the study. The constitutive model is examined in view of the confining stress induced by the lateral steel on the core concrete and the enhanced strength and ductility of core concrete at the columns' axial capacity. The verified range over which the constitutive model remains valid is clarified under practical stress conditions. The effect of loading rate on the plasticity evolution is also discussed.

Keywords *: Confinement, lateral reinforcement, strength, ductility, constitutive laws*

T.M. Pallewatta is Structural and Construction Engineer of Design Consortium Limited, Colombo, Sri Lanka and a former graduate student in the Department of Civil Engineering at the University of Tokyo.

P. Irawan is Assistant Lecturer in the Department of Civil Engineering at the University of Tokyo. His research is in the mechanical behavior of concrete under triaxial confinement and the non-linear analysis of reinforced concrete shells.

K. Maekawa is Professor in the Department of Civil Engineering at the University of Tokyo. His research interests cover reinforced concrete mechanics, computational approach to seismic behavior of reinforced concrete-soil systems, thermodynamics of cement-concrete composites, and durability design of concrete structures.

1. INTRODUCTION

The enhanced axial performance of concrete under passive lateral confinement provided by lateral steel has been investigated for the beneficial it has on the ductility and capacity of members. Design formulas (macro models) have been proposed for peak stress and strain at the peak stress of confined concrete[1),2)]. These do not directly consider the microscopic aspects of confinement, but rather have been developed through an empirical approach which represents experimental facts of practical interest.

A recent development is the introduction of 3-dimensional constitutive models for local points in confined concrete and other computational tools that enable stresses, plasticity, and damage fields arising in real members to be computed with less effort[3)]. These simulations can in turn be used to check the validity of microscopic models of concrete. In fact, to obtain universal computational tools, experimental verification is most crucial at the member level, where there is a non-uniform stress field[4)]. Though data on the capacity of confined concrete columns are abundant, there are very few articles of use in the experimental verification of microscopic constitutive models.

To fill this gap, verification-oriented idealized experiments were conducted for the following four cases: 1) no concrete cover to avoid a non-confined zone; 2) closed loop welded ties designed for perfect anchorage of lateral reinforcement; 3) round bars used to eliminate bonding and to measure strain over the whole zone; and 4) no longitudinal bars to avoid load carrying mechanism of steel. The crucial engineering point is to experimentally identify induced the "real confining stresses" which are related to the strength enhancement of the core concrete. These stresses are also used to verify micro-models. As already stated, the main aim of this study is to obtain reliable data for verification of 3D constitutive laws for concrete[5)] at the member level through a computational approach.

The stress-strain behavior of concrete comprises non-linear ascending and descending branches. In the strain softening area, compressive strain measurements are greatly affected by the loading rate and specimen size due to strain localization. Since the major objective of this study is to obtain systematical data for the verification of constitutive laws, we focus first on the ascending branch, which portrays the pre-peak behavior and can be obtained with higher precision.

2. CONFINEMENT EFFECTIVENESS INDEX

Three-dimensional stresses in core concrete are non-uniform except in cylindrical cores confined by hydraulic pressure or a steel cylinder. Consequently, indexes to represent the confinement effectiveness of lateral ties arranged in three dimensions under non-uniform stress fields are needed and must also be experimentally identified. The authors have introduced three indexes defined at a local point, a section, and the entire volume of a concrete member, respectively[3)].

The reference system is such that the x and y axes lie in lateral orthogonal directions while the z axis is along the axis of the confined core, as shown in **Fig. 1.** The lateral confining stress at a point (x,y,z) is defined as the in-plane first invariant (Eq.(1)) of lateral stress. By integrating this over the domain of the (x-y) cross-section, the *sectional average confining stress* denoted by $\overline{\sigma_c}$ is obtained as,

$$\sigma_c \equiv \frac{\sigma_{c,xx} + \sigma_{c,yy}}{2} \tag{1}$$

$$\overline{\sigma_c} = \overline{\sigma_c}(z) = \frac{1}{A_c}\int_{A_c} \sigma_c(x,y,z)\, dx\, dy \tag{2}$$

where, A_c is the domain of the cross section and $\sigma_{c,ij}$ is the concrete stress tensor.

Further integration of the sectional average confinement along the axis of the core results in the *spatial average confining stress* denoted by σ_v, which is the volumetric average of the lateral confining stresses induced in the concrete:

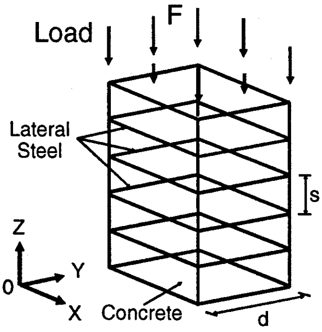

Fig.1 Confined concrete core

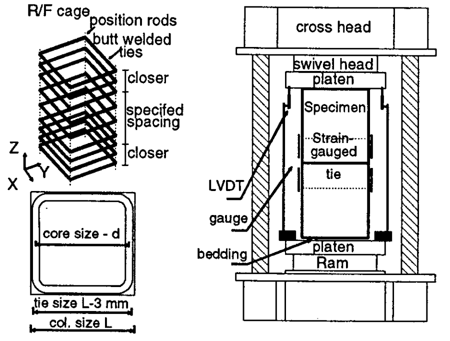

Fig.2 Specifications and experimental setup

$$\sigma_v \equiv \frac{1}{H}\int_H \bar{\sigma}_c \, dz = \frac{1}{V_c}\int_{Vc} \frac{\sigma_{c,xx} + \sigma_{c,yy}}{2} dV \tag{3}$$

where, V_c is the volume domain of the core while H is the length in the z-direction of the core enclosed by hoops.

By applying the virtual work principle, the equilibrium condition existing between confining steel and confined core can be proven[3] as Eq.(4), where σ_s and V_s are the steel fiber stress along the axes of lateral reinforcing bars and the steel volume, respectively.

$$\sigma_v = -\frac{1}{2V_c}\int_{V_s} \sigma_s dV \tag{4}$$

The relation represented by Eq.(4) is of great importance since the averaged confining stress is equated to the spatially averaged steel stress integrated over its domain. This quantity reaches a peak, reflecting the maximum level of confinement that can be generated, when all the steel reaches yield. This limit condition is depicted in Eq.(5), where p is the volumetric lateral reinforcement ratio and f_y is the yield strength of the steel.

$$\sigma_{v,\lim} = -\frac{1}{2}\left(\frac{V_s}{V_c}\right) f_y = -\frac{1}{2} p \cdot f_y \tag{5}$$

The ratio of actual confinement as denoted by Eq.(4) and the maximum attainable as denoted in Eq.(5) is used to indicate the mechanically defined confinement effectiveness of a particular detailing, as given in Eq.(6), and will be referred to as the *confinement effectiveness index*. This newly introduced index quantifies confinement effectiveness on a theoretical basis. Further, the possibility of experimentally obtaining this index opens the way to the verification of numerical models of materials as well as structures.

$$\alpha = \sigma_v / \sigma_{v,\lim} \tag{6}$$

From the above discussion, it is clear that if a 3D axial stress distribution can be obtained for the confining steel in the whole domain, then the spatial average confining stress applied to the concrete can be computed. In order to obtain the axial stress distribution in the confining steel, strain measurements at discrete locations along a tie on two extreme fibers at each location need to be carried out. With information about the stress-strain relation of the steel and using the "*plane section hypothesis*", the stress distribution across the tie cross section can be computed. Through such discrete measurements along tie arms, the average 3D confining stress can be experimentally computed using Eq.(4).

Table 1 Detail of experiments

Designation and Comments	Column Size (L) (mm)	Tie Diameter (Ø) (mm)	Core Size (d) (mm)	Tie Spacing (s) (mm)	Reinforcement ratio (p) (%)	Spacing ratio (s/d)
C16-075, High r/f	200	15.70	181.3	75	5.70	0.41
D19-104, High r/f	200	18.70	178.3	104	5.92	0.58
O19x2-232, High r/f	200	18.80	178.2	232	5.37	1.20
A09-042, Medium r/f	200	9.00	188.0	42	3.22	0.22
H133-094, Medium r/f	200	12.95	184.1	94	3.05	0.51
I16-150, Medium r/f	200	15.85	181.2	150	2.91	0.83
J19-225, Medium r/f	200	18.80	178.2	225	2.77	1.26
M09-090, Low r/f	200	9.00	188.0	90	1.50	0.48
N13-192, Low r/f	200	12.95	184.1	192	1.49	1.04
P09-043, Size Effect Small Core	150	9.00	139.0	43	4.26	0.31
S25-119, Size Effect Big Core	400	24.80	373.2	119	4.35	0.32
T13-065, Size Effect Flex. Effect	200	12.95	184.1	65	4.40	0.35
U13-065-C, Corner Action, Flex. Effect	200	12.95	184.1	65	4.40	0.35
V16-075-LS, High r/f Low conc. Strength	200	15.85	181.2	75	5.81	0.41

3. EXPERIMENTAL APPROACH

3.1 Specifications

Square concrete columns with discrete lateral reinforcement and no longitudinal reinforcement nor cover concrete over the lateral ties were selected so as to give simple and clear boundary conditions. These columns are beneficial for experimental verification of computational models. Along with the reinforced specimens, plain concrete columns of the same dimension were cast to obtain the unconfined capacity for comparison.

The same grade of steel was used in all experiments and the yield strength was within a narrow range for different bar diameters. The confined concrete core is here defined as the volume bound by the centerlines of the peripheral ties, as shown in **Fig.2.** Series of experiments were carried out to investigate 1) the size effect for cores with the same reinforcement ratio ($p \approx 4.5\%$) and the same spacing ratio ($s/d \approx 0.3$: See **Fig.1.**); 2) the effect of lateral reinforcement ratio and spacing with the same grade of steel; and 3) the effect of tie arm flexural stiffness, achieved by separating the core concrete from the tie arms except at corners. In these tests, higher reinforcement ratio samples are compared with actually constructed columns in order to obtain data over a wide range so as to verify the constitutive model. Detailing parameters are summarized in **Table 1.**

3.2 Fabrication

The lateral reinforcement consists of square hoops formed from plain round bar as shown in **Fig.2.** In reality, the anchorages at the two ends of each bent bar forming a tie would significantly affect the lateral confinement performance. Since uncertain boundary conditions would result in data that would make verification of the computational model infeasible, it was decided to form closed lateral ties by complete welding. Butt welding was carried out and the facing edges were chamfered. A filler metal was used to bridge the gaps, resulting in a continuous tie section instead of an enlarged lap at the weld.

Ties were fabricated to very close tolerances in order to achieve high accuracy in the experimental results. A clearance of 1.5 mm per side between the outer dimension of the ties and the steel formwork was allowed for

Table 2 Mix proportion of self-compacting concrete

Mixture	Water (kg/m^3)	Cement (kg/m^3)	Sand (kg/m^3)	Gravel (kg/m^3)	Ad-mixture (%)	Slump flow (cm)
	185	520	850	899	2	58

Maximum size of aggregate : 20mm

mounting and insulating the external fiber strain gauges. Bending was carried out such to a tolerance of ± 1mm against the specified dimensions. Mild steel hot-rolled plain reinforcement bars were used, allowing welding without any localized normalizing effects due to the elevated temperatures.

To ensure that the critical section (the targeted test domain) for axial failure would be around the center of each column, ties were placed closer together near the two ends of each column.

3.3 Selection of concrete

Material uniformity was crucial in these experiments since member failure is governed by the weakest section under axially uniform stress fields. Since there is no cover, shrinkage must be avoided since it causes concrete to separate from the ties. This leaves gaps resulting in premature failure. Bleeding and segregation should also be minimized to prevent any initial weak zones in the upper portions of castings.

In order to satisfy the above conditions, a self-compacting high-performance concrete[6)] was utilized throughout the test program. All specimens were cast in a horizontal position so as to form moulded loading ends, promote better filling of restricted locations, and facilitate the routing of strain gauge wires. Each specimen was cast with a single mix proportion in a continuous operation. The mix is listed in **Table 2.**

3.4 Instrumentation and testing

Axial mean strains were measured in the critical region of each column -- the section influential in the load carrying mechanism -- by π-type gauges mounted on cross rods integrally cast into the column. These rods were located symmetrically around the central ties. Displacements between the loading platens were also measured at the four corners of the column by linear variable displacement transducers (LVDT), as shown in **Fig.2**. This measurement merely serves to monitor platen parallelism during loading and as cross check for axial strains.

The measurement of tie strains across and along tie arms using strain gauge pairs – as a means of obtaining a strain distribution that can be converted to a stress distribution and spatial average stresses --, is the distinguishing feature of this experimental method. Continuous measurement of strain variations using as many strain gauge pairs as possible is desirable. In practice, however increasing the number of strain gauges results in increased voids between steel and concrete. Given this limitation, five pairs of strain gauges were used per tie arm as shown in **Fig.3**.

Proper bedding between specimen ends and machine platens was achieved by applying a very rapid hardening cement grout layer between the loading ends and the machine platens. This bedding operation was performed at the same time as adjustments for concentricity of loading. A loading rate of 3-5 μ/sec in axial strain was maintained from elasticity to the non-linear zone. Loading was generally continued beyond the peak until the load carrying capacity fell at least to 80% of the maximum.

3.5 Experimental data processing

The concrete core is assumed to be bound at the tie centerlines. Though the concrete cover over the ties was intentionally eliminated, same concrete inevitably remains outside these center lines (i.e. between the tie center lines and their outer edges). The thickness of this concrete portion depends on the diameter of the tie bar. Since this concrete cannot be categorized as part of the core, its load carrying effect was assumed to be similar to that of unconfined concrete[7)-11)].

The load assumed to be carried by the outer layer of unconfined concrete is subtracted from the total load to give the load carried by the core and the core concrete stress.

Table 3 Effect of core size

Designation	Confinement capacity $1/2pf_y$ MPa	Confinement core peak (σ_v) MPa	Confinement effectiveness index by (α)	Unconfined strength (f_{co}) MPa	Core peak strength (f_{cc}) MPa	Strain at core peak (ε_{cc}) (micro)
P09-043 - small	7.13	6.38	0.90	38.0	53.0	10535
S25-119 - large	6.61	5.63	0.85	37.3	51.4	10386
T13-065 medium	7.22	6.56	0.91	36.7	51.8	10974

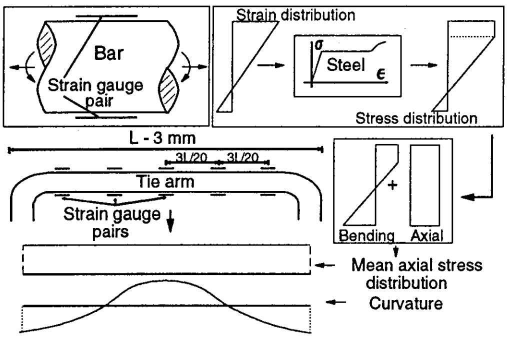

Fig.3 Spatial stress measurement in lateral reinforcement

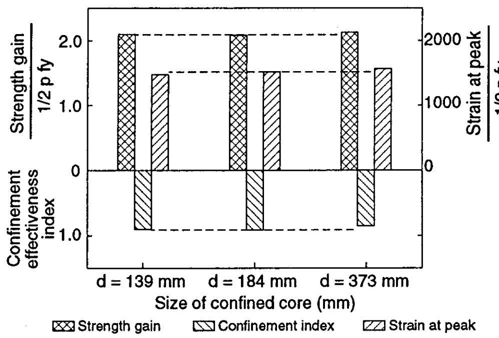

Fig. 4 Core size effect on confinement

The strain in extreme fibers of the steel ties was measured and, based on Kirchoff's "plane-section hypothesis," the strain distribution was obtained for the whole section. With knowledge of the steel's stress-strain properties obtained in advance, the sectional fiber stress at each location is computed from the strain reading. Here, the mean strain at a location is obtained by averaging the strain of the two extreme fibers, while their difference divided by the bar diameter results in the curvature. Since strain gauges were located at equal intervals along tie arms and the ties had a uniform diameter, averaging the mean stresses obtained at individual locations over the length of a tie arm results in the steel stress averaged over its domain. Using this average, the spatial average confining stress of the concrete core (σ_v) is obtained by Eq.(5). This value is of main point of this study.

3.6 Confinement Effectiveness of Lateral Reinforcement

(1) Size of concrete core

To isolate the size effect on confinement effectiveness up to the ultimate capacity, other factors with an influence on confinement were kept constant while changing the core size. For the purpose of this study, three specimens with outer sizes of 150, 200, and 400mm were utilized. The lateral reinforcement ratio (p=4%), spacing ratio (s/d =0.32), steel yield strength, and unconfined concrete strength were kept nearly constant.

The specimens used for this comparison and the results are compiled in **Table 3**. For this series of experiments, results for peak core strength are presented in the form of confinement effectiveness index, strength gain, and strain at peak core strength, all normalized by potential available confinement (*½pf*$_y$) in **Fig.4**. This normalizing accounts for the slight variations in potential available confinement. It is clear from this figure that, for the core sizes investigated, all three quantities are virtually constant.

Table 4 Effect of reinforcement content and spacing

Designation	Confinement capacity $1/2pf_y$ MPa	Confinement core peak (σ_v) MPa	Confinement effect index (α)	Unconfined strength (f_{co}) MPa	Core peak strength (f_{cc}) MPa	Strain at core peak (ε_{cc}) (micro)
C16-075	9.49	7.64	0.80	36.9	59.5	12655
D19-104	9.24	7.20	0.78	35.6	53.4	9449
O19x2-232	8.49	1.72	0.20	35.2	39.0	2734
A09-042	5.40	5.06	0.94	35.6	46.3	7187
H13-094	4.99	3.67	0.73	35.6	43.9	5371
I16-150	4.56	2.11	0.46	35.6	42.6	5660
J19-225	4.38	1.07	0.24	35.6	39.9	3642
M09-090	2.52	1.80	0.71	35.2	40.3	4439
N13-192	2.45	0.64	0.26	35.2	37.7	2330

It can be concluded that, within this range, the size of the core has no significant influence on confinement in the peak state. This conclusion is significant since it means parametric studies can be conducted on small-scale specimens to identify the effect of other significant variables.

(2) Reinforcement ratio and spacing

The amount of lateral reinforcement has often been adopted as a parameter in previous studies. Here, it is considered in terms of the volumetric ratio of lateral reinforcement. Further, the spacing of lateral reinforcement is addressed using the concept of a dimensionless spacing ratio, which takes into account both core size and lateral reinforcement spacing. It was found that the core size does not have a significant bearing on confinement effectiveness, if this normalized spacing ratio is used to represent the detailing of lateral reinforcement.

During this series of experiments, the point is to keep the maximum confinement (the potential for introducing confinement to the core concrete by the lateral steel : $\frac{1}{2}pf_y$) constant while varying the normalized spacing ratio. For all experiments, the same grade of steel was used and the yield strength varied little. This means that the volumetric lateral reinforcement ratio can be treated as a direct indicator of potential confinement capacity in our discussions. Three reinforcement ratios referred to as high ($p \approx 6\%$), medium ($p \approx 3\%$), and low ($p \approx 1.5\%$) were studied (See **Table 1**). The confinement and strength results for this series are given in **Table 4**.

The mean axial stress and average spatial confining stress are plotted against mean axial concrete strain for the medium reinforcement ratio ($p \approx 3\%$) for different normalized spacing ratios in **Fig.5** through **Fig.8**. It can be seen from these figures that, in all cases, the resulting confining stress with respect to axial loading is low at first and increases later. Initially, the lateral expansion is lower but, as the stress on the core increases, damage within the concrete causes lateral expansion to increase at a higher rate.

However, in efficiently confined cores with smaller spacing, where high confining stresses closer to potential are generated, the rate again falls. This is due to non-linearity in the confining steel caused by localized yielding coupled with the anisotropic non-linearity of the core concrete. Since the behavior of confined concrete at the core peak strength is the prime interest in this study, the confinement developed at this level is addressed in detail below.

The variation in spatial average confining stress (σ_v) with normalized lateral reinforcement spacing ratio is given in **Fig.9,** from which it can be seen that an increase in lateral reinforcement results in an increase in absolute averaged confining stress. A clear reduction in confinement effect with increasing normalized spacing ratio is observed for all reinforcement ratios[3)].

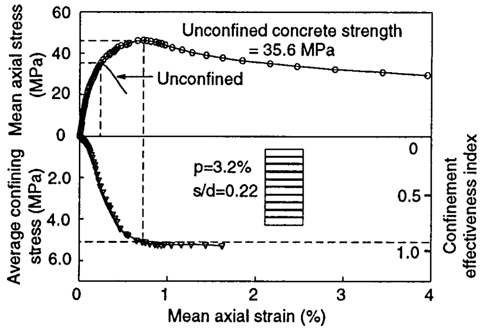

Fig.5 Stress-strain, confinement :s/d=0.22 -specimen A09-042 -

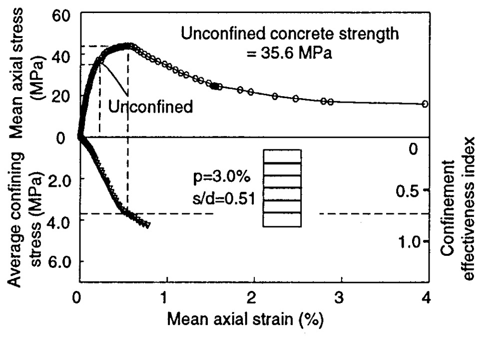

Fig.6 Stress-strain, confinement : s/d=0.51 - specimen H13-094 -

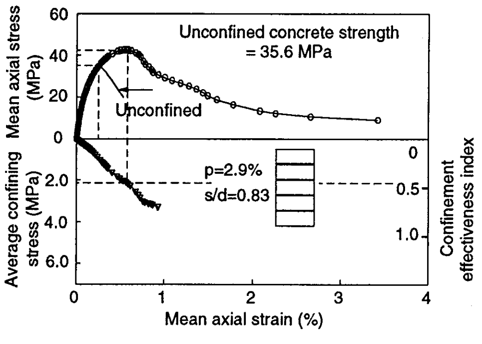

Fig.7 Stress-strain, confinement : s/d=0.83 - specimen I16-150 -

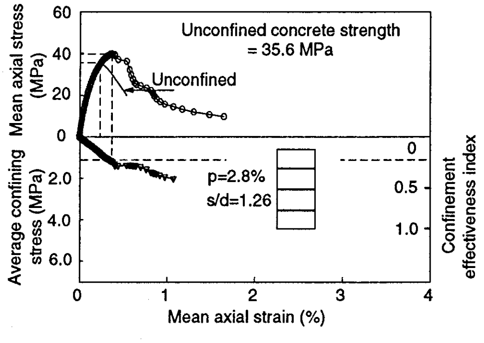

Fig.8 Stress-strain, confinement : s/d=1.26 - specimen J19-225 -

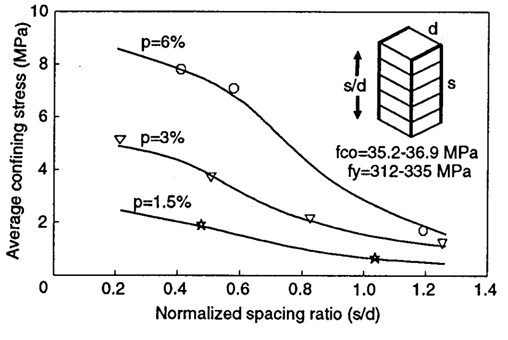

Fig.9 Average peak confinement in core

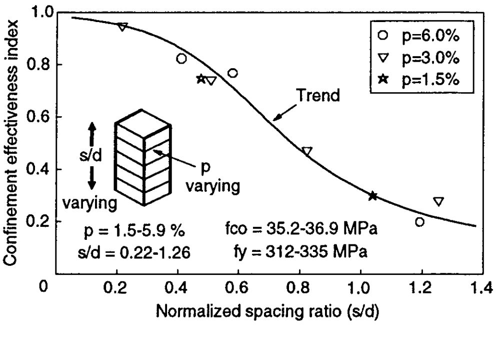

Fig.10 Confinement effectiveness index against spacing ratio

The variation in confinement effectiveness index with normalized spacing ratio for the different volumetric reinforcement ratios is given in **Fig.10**. In the case of smaller spacing, almost all the lateral reinforcement yields (the index ≅1.0) but a larger spacing brings about partial yielding or complete elasticity of the lateral ties (the index <0.6). This means that the experimental series listed in **Table 1** covers a wider range of lateral tie confinement effectiveness, as shown in **Fig.10**. It is interesting to note that the data for different reinforcement ratios follows a common trend. Clearly, the general tendency for lower confinement efficiency with increasing spacing is confirmed.

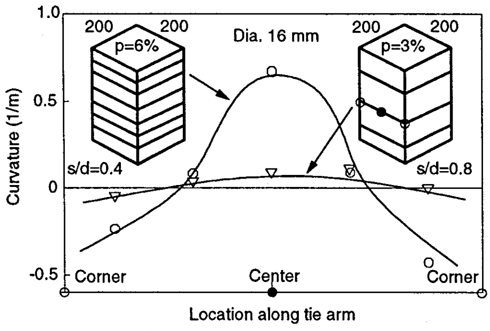

Fig.11 Curvature profiles for ties of the same diameter (C16-075 and I16-150 in Table 1)

These observations on induced confinement and the confinement effectiveness index can be rationalized: the greater spacing leaves a longer length of unsupported concrete between ties, though theoretically the same maximum confinement potential is present. In this passively confined state, the stress developed in the confining agent depends on the ability of the confined concrete to transfer the stress to it. A wider spacing causes degraded uniformity in the internal stress field resulting in higher local damage between ties[3]. This in turn culminates in the concrete being unable to develop greater confining stresses in the steel.

(3) Flexural stiffness of lateral ties

If the lateral ties act merely as truss agents, confining stress can only be induced by the tie corners into the core concrete. Though this corner action will be predominant for smaller bar diameters, larger bars associated with higher flexural and shear stiffness may induce additional confinement through the entire contact interface between lateral ties and concrete.

This can be checked by looking at the curvature of the tie arms as obtained from the experimental strain measurements. Curvature profiles for ties arms are shown for a pair of columns at their respective peak strengths in **Fig.11**. The columns compared have the same core and bar size but the spacing in the column which develops greater curvature is half that of its companion, while the reinforcement ratio is double. This indicates that with closer spaced confining arrangement the curvature induced in the bar increases. The increased lateral restraint leads ultimately to greater lateral deformation of the concrete, which is closely related to the curvature of lateral ties.

These observations indicate that different bending moments and shear forces are acting in the reinforcing bar sections. The induced moment must be in equilibrium with the contact force acting on the core concrete. This contact force enhances confinement along the tie arms as well as the corner action resulting from axial forces on the bars between core corners. To investigate on this, a special experiment was designed to eliminate the transfer of forces from steel to concrete by removing all contact, except at the corners. This experiment was also intended to serve the purpose of verifying microscopic analysis.

Brudette and Hilsdorf conducted similar tests by using four steel angles secured by bolts to plain concrete square columns[12]. The contact between angles and column corners were filled with mortar. To reduce the axial load transferred to the angles by friction, teflon strips were inserted between the angle and mortar fill. The reduction in contact stiffness caused by the mortar fill and teflon strips, which leads to poor stress transfer across the corners, is the cause of the scatter in the observed data. With this uncertain boundary condition, it would be difficult to use this data for verification of the constitutive laws and FEM 3D analysis.

For the purpose of this study, a different method was adopted. Ties were separated from the core concrete by adding a deformable layer to prevent transfer of contact forces. The length of the corner contact regions was chosen on the basis of the maximum size of coarse aggregate. Concrete outside the tie centerlines was eliminated by placing polystyrene layers between the ties. The specifications of this special experiment are

Table 5 Effect of flexural stiffness of lateral bars

	Limit confinement 1/2pfy	Confinement. Peak by σ_v	Effectiveness index by α	Unconfined strength	Peak strength	Peak strain
T13-065 beam effect	7.22 MPa	6.56 MPa	0.91	36.7 MPa	51.8 MPa	10974 micro
U13-65-C corner effect	7.22 MPa	3.15 MPa	0.44	35.8 MPa	41.1 MPa	6205 micro

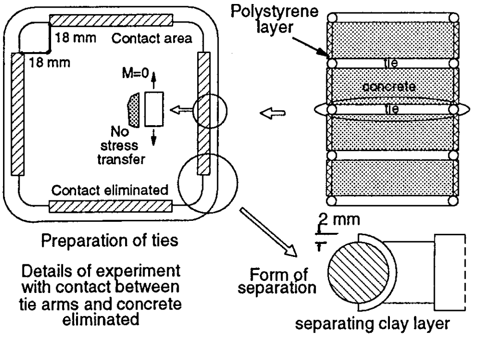

Fig.12 Specifications for corner action test

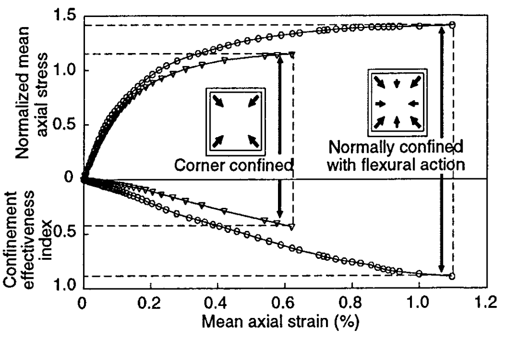

Fig.13 Stress-strain and confinement for corner and contact cases

given in **Fig.12.** The thickness of the deformable layer was kept low so as to minimize the effect of the reduced core area. Observed curvature at the tie center was nearly zero in the ascending portion of the stress-strain diagram. However, it must be reported that some contact took place after the peak due to geometrically large dilatancy of the core concrete.

To provide a comparison with the above experiment, a control specimen with equal lateral reinforcement ratio, spacing ratio, core size, tie size, and reinforcement strength. In this specimen, contact between concrete and the lateral reinforcement was maintained throughout. Almost the same unconfined concrete strength was attained. The results of the two tests are shown in **Table 5**.

In both cases the maximum potential confinement is the same, but it is clear from **Fig.13** that the corner-confined column develops considerably less confinement stress at the core peak as compared with the normally confined specimen. The mean axial stress normalized by unconfined concrete strength and confinement effectiveness index as plotted against mean axial strain in this figure indicate a definite loss in peak axial strength of the core. The axial strain at peak strength is also seen to be reduced by more than 40% due to the absence of contact. Further, the developed confinement is about 50% of the equivalent normally confined column.

It can be concluded that the flexural stiffness and contact contribution made by the tie arms play a substantial role in enhancing confinement effectiveness. This factor may not be significant in cases of confinement with ties of lower stiffness when the reinforcement ratio is low. However, it is especially significant in cases of higher reinforcement ratio with bars of larger diameter as compared to the core size. In our analytical studies on confinement, including the micro-mechanical model developed from FEM studies, the beam action as well as corner action should be taken into account.

3.7 Enhanced Capacity by Lateral Reinforcement

In this study, the emphasis is on enhancing the peak strength of the concrete core. This is significant since it reflects on structural reliability and soundness. Furthermore, from an engineering point of view, the

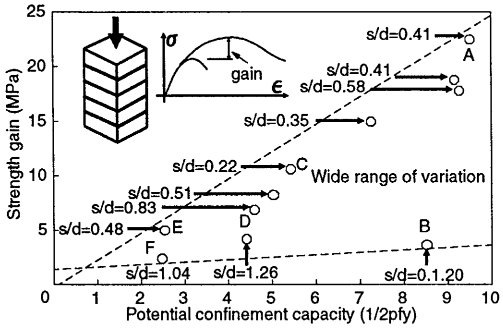

Fig.14 Strength gain and potential confinement capacity at peak core strength

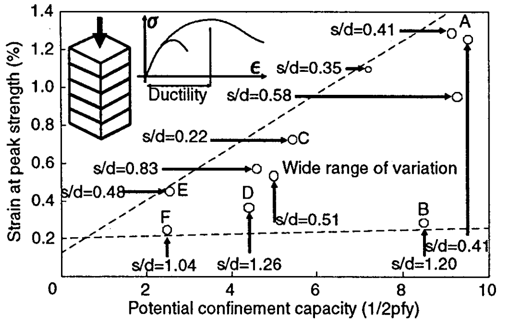

Fig.15 Ductility and potential confinement capacity at the peak core strength

maximum load carrying capacity of a concrete column is of great importance where members are subjected to higher axial forces and combined bending. The axial strain at peak strength is also addressed here.

(1) Capacity gain and reinforcement ratio

It has been assumed by some previous researchers that the strength gain achieved by lateral reinforcement is proportional to the product of reinforcement ratio and steel yield strength[10),11)]. It is interesting to note that this product divided by two represents the potential maximum confinement, denoted by $\frac{1}{2}pf_y$. The assumption may be approximately correct for closely spaced lateral reinforcement, such as with circular columns[3)]. For square columns, however, the validity of the assumption must be verified since this condition is only realized when all the steel yields at the core peak strength. In fact, 3D FEM analysis of square columns subjected to axial compression indicates that steel lateral ties remains elastic even when the axial concrete capacity is reached[3)].

In order to check whether this assumption is indeed correct, the strength gain over the experimental range is plotted against maximum potential confinement in **Fig.14**. Since the steel strengths used in this study vary little, the figure is discussed on the basis of reinforcement ratio. The first thing to note is that the figure indicates a considerable overall scatter. At lower reinforcement ratios, the scatter is about 50% for the higher strength specimen (points marked *E* and *F*). As the reinforcement ratio increases, a very prominent scatter develops. This is confirmed by points *C* and *D*, which represents medium reinforcement ratios, while points *A* and *B* for high reinforcement ratios show the widest scatter. From the spacing ratios indicated at each data point, a clear trend toward greater strength gains for closer spacing at a given reinforcement ratio can be seen. The axial strain at potential peak strength also exhibits a very similar scatter, as seen in **Fig.15**, which depicts peak strain against maximum potential confinement capacity.

This discussion makes it very clear that there exists no direct relation between the volume of steel provided and the strength gain, or ductility, for square columns. The above observations indicate that tie spacing has a strong influence, as previously pointed out. Thus, strength enhancement has to be studied using two main parameters: the amount of reinforcement and the spacing of this discrete reinforcement.

(2) Actually induced confinement

The spatial average confining stress induced by the steel, which is the actually induced confinement, is found to be dependent on the spacing of lateral ties and should be a better parameter for relating to strength enhancement. To examine this relation, **Fig.16** is plotted to show strength gain against the actually induced confining stress at peak core strength for different reinforcement and spacing ratios. Comparing this with the data points discussed in **Fig.14** indicates a more linear relation with less scatter. Point *B*, which was almost directly below point *A* in **Fig.14**, has moved quite close to the origin in **Fig.16**. Also, point *D* in **Fig.14**, which was close to point *C*, has moved closer to the origin. The same can be said for points *E* and *F*. The movement of these points indicates that the new parameter (the actually induced average confinement) is a better

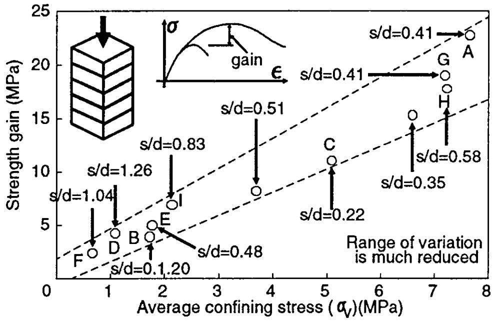

Fig.16 Core strength gain with induced average confining stress at peak strength

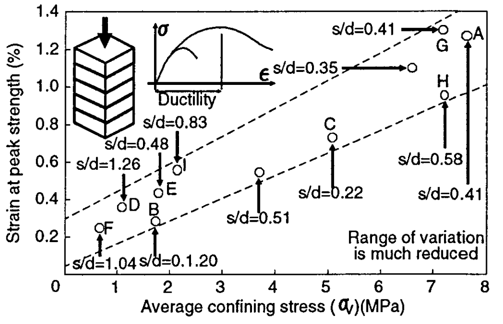

Fig.17 Core strain with induced average confining stress at peak strength

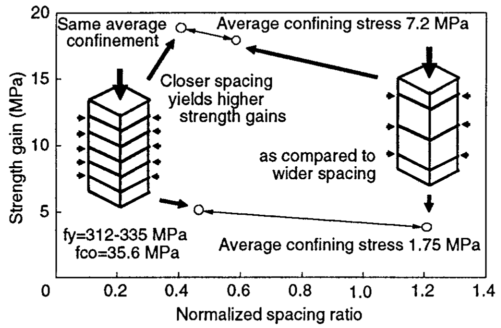

Fig.18 Strength gain at same average confining stress

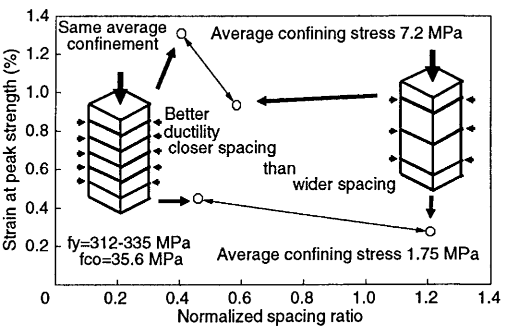

Fig.19 Strain at peak strength at same average confining stress

indicator of strength gain. From a rational view point, also the actually induced confinement should be related to the strength enhancement due to confinement.

Figure 17 relates the axial strain at peak strength to the induced confinement. In this figure, also, the relative positions of points *A-B*, *C-D*, and *E-F* show a similar trend to that observed in the strength gain comparison. Since the confinement effectiveness index is related directly to the induced averaged confinement, this index should offer a good representation of the strength enhancement efficiency due to confinement. In a rational design formula, this index should be evaluated empirically or analytically; however, there is little research data giving actually induced confinement from steel to core concrete. Thus, an analytical approach which has been systematically checked through the use of verification data would be a powerful tool for formulating the confinement effectiveness index in general cases.

Nevertheless, the data still has a lower but significant scatter. This could be attributable to experimental errors. However, if we consider the two sets of data *E, B* and *G, H* in **Fig.16**, each pair has nearly the same induced confinement whereas the strength gains are not equal. This effect is much more pronounced when the same two pairs of points are compared in **Fig.17**. It is very clear from the two figures that points *E* and *G*, as compared to points *B* and *H*, show greater strength gain as well as ductility. This observation tends to suggest that a further influencing factor may exist that has not yet been accounted for.

(3) Double effect of spacing to core size ratio

It was observed above that two sets of results with nearly the same induced spatial average confining stress developed different strength gain and ductility. When the detailing parameters of the two pairs of specimens were checked, it was realized that the higher strength gain or ductility was developed in the specimens with

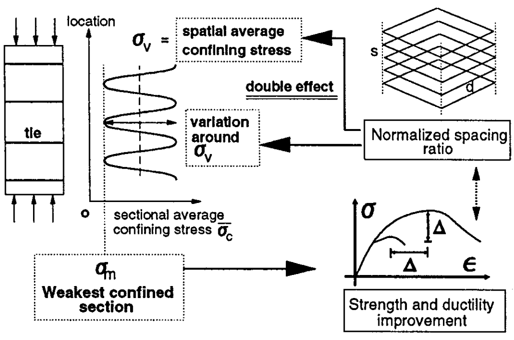

Fig.20 Double effect of reinforcement spacing

closer spacing. This suggests that the spacing has a second effect on strength enhancement due to confinement. This observation is presented in **Fig.18** for strength gain and in **Fig.19** for strain at peak strength.

Since sectional confining stress varies along the axis of the column, even where the volumetric average stress is the same, a column with wider spacing will show more variation than the one with closer spacing. Rationally, it can be assumed that the confining stress in the least-confined section (i.e. midway between the ties), governs the peak strength and corresponding ductility. Based on this assumption, the wider-spaced column exhibit a lesser strength gain and ductility as compared to a close-spaced specimen, even if the same volumetric confining stress is induced in the concrete core.

This finding is quite significant since it directly implies that the spacing of lateral ties has a double effect on the enhancement of capacity due to confinement. In previous studies, this second effect has not been observed since the induced confinement was not comprehensively measured. The extensive strain measurements on ties aimed at computing the average confining stress made this discovery possible.

The first effect of spacing is significant when the induced average confining stress is considered; the ability of steel to resist the expansion of concrete is supplemented when the spacing is reduced. This in turn results in the expanding concrete inducing higher stresses in the steel domain. Such induced stresses in the steel are transferred back into the concrete in the form of confinement spread over the whole concrete volume.

The second effect determines the weakest confined section according to the distribution of this induced confinement along the column axis. Since the section with the lowest confinement should govern the strength enhancement of the member, wider-spaced detailing should result in a lower level of strength as compared to a closely spaced case, even if the spatial average confinement is the same. The influence of the main parameters on confinement is depicted in **Fig.20**. An analysis based on micro mechanical models can be used to verify the arguments put forward in this section.

4. VERIFICATION OF 3D CONSTITUTIVE MODEL OF CONCRETE

Computational mechanics has gained considerable popularity owing to its versatility in the treatment of actual structural member behavior. The attractiveness of the approach lies in its wide applicability to different configurations, boundary conditions, and loading conditions. Here, one of the most important factors for obtaining accurate results is the installation of reliable constitutive laws of the materials[13),14)].

Though concrete cannot be strictly categorized as a continuum due to micro discontinuities, it can be considered, when averaged over a finite region, to be a continuum. Using FEM, it is then possible to simulate concrete structural behavior, provided that the constitutive relations incorporated are sound representations of the concrete itself. One of the constitutive models for concrete is the combined elasto-plastic and continuum fracture model[15)]. The original model, developed for 2D stress states, has been enhanced to represent three-dimensional non-linearities in concrete[5)]. The model was developed and verified at material level under uniform stress fields in the hardening stage.

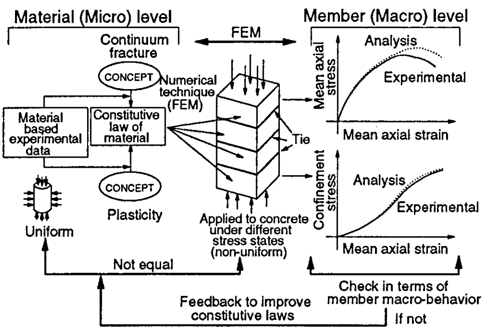

Fig.21 Constitutive law and verification

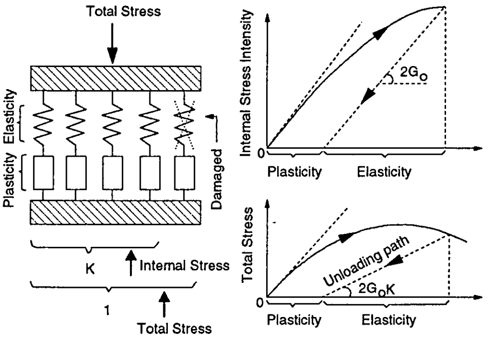

Fig. 22 Elasto-plastic and continuum fracture concept

It is essential to further examine the applicability of any constitutive model under non-uniform stress fields and the realistic stress paths generally encountered in actual reinforced concrete engineering problems[4]. For this purpose, the authors applied the constitutive model, using FEM, to the problem of three-dimensional non-linear behavior of concrete columns under passive confinement imparted by lateral reinforcement in the ascending part of the stress-strain relation.

In doing this, reliable experimental results with simple and clear boundary conditions and systematically arranged parameters are crucial. To obtain these, a test program in which square concrete columns confined with square perfectly closed ties without longitudinal reinforcement nor cover concrete was implemented as described in the previous chapter.

This chapter describes the primary verification of the three-dimensional elasto-plastic and continuum fracturing model for concrete confinement at the member level under non-uniform stress. The range of applicability of this microscopic approach in the ascending branch of the mean axial stress-strain relation is also explained. An outline of this process[4] is illustrated in **Fig.21**.

4.1 Three-Dimensional Analysis of Stress and Damage

(1) Constitutive law of concrete

The constitutive model of concrete used can be schematically idealized as shown in **Fig.22**. The total stress is identified as the assembly of internal stresses developed over the non-damaged elasto-plastic elements. Here, elastic strain is directly proportional to internal stress intensity applied to active non-damaged elasto-plastic elements. Thus, the elastic strain is chosen to represent the internal stress intensity, which governs the plasticity and fracturing of the concrete continuum with defects. An index named the fracture parameter (K) is introduced to represent the ratio of the active volume of concrete able to can carry internal stress. The model basically derives from the four experimental results complied below. Details are discussed in reference 5).

(a) Fracturing in hydrostatic stress state

It is found that the capacity to store volumetric elastic strain energy is not affected by the level of 3D confinement nor by the level of damage induced in the concrete[5]. This means that the entire volume of concrete is active with respect to the volumetric elasticity. **Figure 23** shows that regardless of the level of applied confinement, the relationship between the hydrostatic stress invariant (I_1) and the volumetric elastic strain invariant (I_{1e}) remains constant, and can be mathematically described as[16]

$$I_1 = 3K_0 I_{1e}$$
$$I_1 \equiv \sigma_{kk}/3 \quad I_{1e} \equiv \varepsilon_{ekk}/3 \tag{7}$$

where, K_0 is the volumetric elastic constant and σ_{ij} and ε_{eij} are total stresses and elastic strain tensors, respectively.

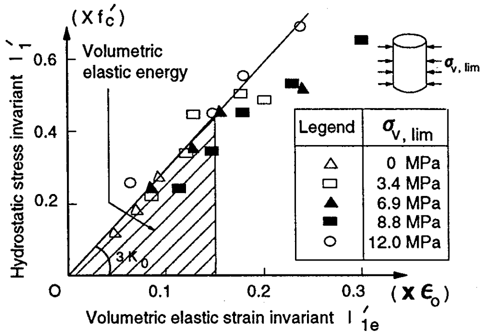

Fig.23 Hydrostatic stress vs. volumetric elasticity

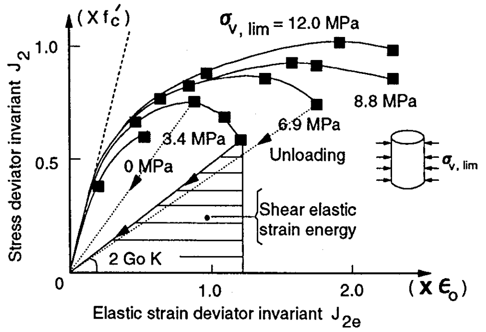

Fig.24 Deviator stress vs. strain invariant

(b) Fracturing in shear

The level of damage caused by shear in the concrete influences the capacity of concrete to store shear elastic strain energy[5]. The continuum damage represented by fracture parameter K develops with internal shear stress intensity, while it is retarded by volumetric confinement. The plot of stress deviator invariant against elastic strain deviator invariant in **Fig.24** shows that the relationship between the two is affected by the level of confinement.

To represent the response of damaged concrete in shear, the relationship between total stress deviator invariant (J_2) and elastic strain deviator invariant (J_{2e}) is adopted in the model as

$$J_2 = 2G_0\, K(F)\, J_{2e}$$
$$J_2 \equiv \sqrt{\sigma_{ij}\cdot\sigma_{ij}/2} \qquad J_{2e} \equiv \sqrt{\varepsilon_{eij}\cdot\varepsilon_{eij}/2} \tag{8}$$

where, F is a damage measure function of J_{2e}, J_{3e}, and I_{1e}, and G_0 is the initial elastic shear stiffness.

Since the level of fracturing is path dependent, the maximum of the damage measure, F_{max} experienced in the past loading history of concrete is taken as the value of F in Eq.(8). If the updated value of F is smaller than any previous value, the fracture condition is assumed to be stable with no worsening damage. With greater confinement, the propagation of micro defects is restrained. This implies that greater confinement results in a larger fraction of the concrete domain contributing to shear mode resistance at a given shear elastic strain.

It is found that when the fracture parameter K falls below 0.25, compressive strain localization is induced in the concrete. Here, the strain field is no longer uniform and absolute strain is size-dependent. Thus, this value is tentatively identified as the applicability limit of the model.

(c) Plasticity in shear

Plasticity in deviatoric shear denoted by J_{2p} is enhanced with increasing internal shear stress intensity represented by J_{2e}. However, it is found that deviatoric plasticity is not influenced by the volumetric confinement, as shown in **Fig.25**. This effect is represented by the plastic hardening function H as[5]

$$J_{2p} = H(J_{2e\max})$$
$$J_{2p} \equiv \int \frac{e_{eij}\, d\varepsilon_{pij}}{2J_{2e}} \tag{9}$$

where, $J_{2e\,max}$ is the maximum of J_{2e} in the past loading history, e_{eij} is the elastic strain deviator tensor, and ε_{pij} is the plastic strain tensor. If the updated value is lower than any previous value, the plasticity is assumed to

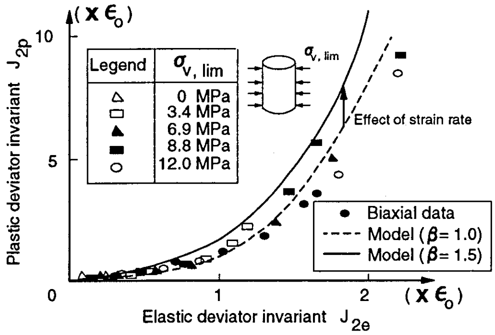

Fig.25 Plastic progress in shear mode

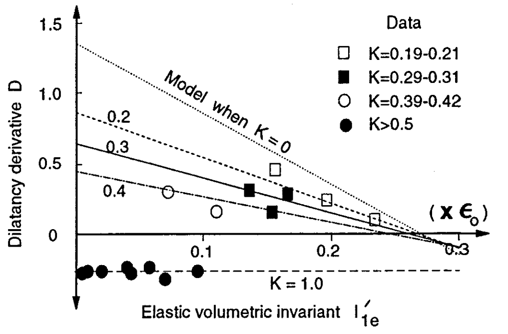

Fig.26 Dilatancy derivative

be unchanged. Based on uniformly confined experiments, a plastic hardening function, ($H=H(J_{2e})$), has been proposed for normal concrete.

Here, it must be remembered that the plastic evolution function was formulated with reference to short-term loading tests on concrete solids[5]. If the stress rate arising in real structures differs from the condition on which the function H was based, we have to take into account time-dependent plasticity in the verification process. In fact, it was reported by Okamura et al.[4] that under 2D states, plastic evolution law for concrete has to be modified in terms of the real loading rate arising in the target structure, and the following simple correction factor is used for cyclic analysis of RC plates:

$$J_{2p} = \beta \cdot H(J_{2e}) \tag{10}$$

where, β=1.5 for laboratory structural experiments.

The authors now discuss the difference in loading rate between the material-based test condition and structural reality with respect to this correction factor. The use of correction factor (β) to take into account the effect of loading rate is in accordance with previous studies on the effect of strain rate on the strength and ductility of plain and confined concrete. It is found that a higher strain rate will increase the strength and ductility of plain as well as confined concrete[17)-19)]. In deriving the model, it takes only several minutes to apply the load to the specimen. On the other hand, several hours are needed in the case of real structures tested in laboratories. This difference in loading time affects the plastic evolution of the concrete and the correction factor is adopted to take into account this effect.

Since time dependent fracturing and damage evolution are reported to be comparatively less affected by the stress rate[4], time dependent fracturing will not be discussed in this study.

(d) Plasticity in volume

The volumetric plastic strain (I_{1p}) associated with shear plasticity (J_{2p}) is significantly affected by the degree of confinement[5]. This non-linearity, named *shear dilatancy*, is represented by the dilatancy derivative (D) given in Eq.(11) and Eq.(12).

$$dI_{1p} = D(I_{1e}, K)dJ_{2p} \tag{11}$$

$$dI_{1p} = \tfrac{1}{3}d\varepsilon_{pkk} \tag{12}$$

Based on experimental data, the *dilatancy derivative* ($D=D(I_{1e}, K)$) has been formulated[5] as shown in **Fig.26.** An increase in confinement causes this expansion or dilatancy to fall.

Since the progress of volumetric plastic strain is gradual and depends on the level of damage in the concrete and the applied confinement, dilatancy derivative (D) is written as a continuous function,

$$D = D_0 K^2 + D_1 (1-K)^2 \tag{13}$$

The effect of Poisson's ratio and confinement is taken into account in D_o and D_1, respectively[5].

The four relations and equations given above are the core of the three-dimensional continuum fracture and plasticity constitutive law. By solving these simultaneous equations, we obtain an incremental constitutive equation in terms of total stresses and strains,

$$d\{\sigma\} = [M]\,([I]+[L])^{-1} d\{\varepsilon\} \tag{14}$$

where, $[M]$ and $[L]$ represent the fracture and plasticity matrices, respectively[5].

Since it combines plasticity and fracturing formula, this constitutive model covers strain hardening and softening in a continuous and consistent manner. With greater confinement, the evolution of fracturing in shear is restrained. It coherently makes the overall behavior of concrete more plastic as it should be.

Although the softening behavior can be mathematically dealt with by the model proposed, the authors regard post peak softening as being out of the range of applicability. Material functions and coefficients are formulated independent of element size for simplicity, meaning that the model cannot be applied in general to the strain softening range in which the apparent constitutive relation is greatly size-dependent. Thus, the authors first concentrate on the strain hardening 3D behavior up to the size-independent peak strength even though the model is fundamentally capable of covering the softening zone.

(2) Model of Reinforcement

The steel bars used as lateral reinforcement were modeled using two idealizations as truss members only capable of resisting axial loads and as beam members incorporating flexural and shear stiffness.

In the first idealization as a truss, which is simpler in analytical implementation, a 3D isoparametric element having only axial stiffness and a translational degree of freedom at the nodes was implemented. Since no rotational degree of freedom is modeled, the bending moment and shear force developed along the element cannot be idealized.

In the second idealization, the Timoshenko beam element[20] was selected. In this element, a plane section initially normal to the mid-surface remains plane but not necessarily normal to it. This condition allows transverse shear deformation. Both translational displacement and rotational fields are interpolated along the finite element. This allows flexural stiffness to be taken into account for larger sections of steel bars. Since it involves a shear energy term, the reduced integration scheme proposed by Zienkiewicz[20] is adopted so as to avoid "shear locking". The stress-strain relation assumed for steel is the elastic perfect plastic model.

(3) Finite element idealization

The square member considered in this analysis has axial symmetry which allows us to discretize only a one-fourth portion in the lateral direction as finite elements. In the longitudinal direction, two layers of concrete isoparametric elements with 20 nodes are used dividing the half tie spacing into two. To account for non-uniformity in the lateral direction, four solid concrete elements per layer are adopted as shown in **Fig.27**. This discretization was chosen after conducting preliminary check for mesh size convergence in the hardening stage of the columns concerned.

Loading is accomplished by applying forced axial displacement to the top surface of the concrete. The bottom surface is maintained as a fixed boundary. Computation was conducted in the ascending part of the concrete axial stress-strain behavior in consideration of the mesh sensitivity to compression softening.

One core characteristic adopted for verification was the mean axial stress-strain relation of columns. This relation is a reflection of local plasticity and damage to the concrete in the light of the overall response of the member. The other was the mean confining stress as defined in Eq.(3). This equation represents the degree of confinement actually induced by the lateral reinforcing bars and is closely associated with the plastic dilatancy and continuum fracturing model of concrete.

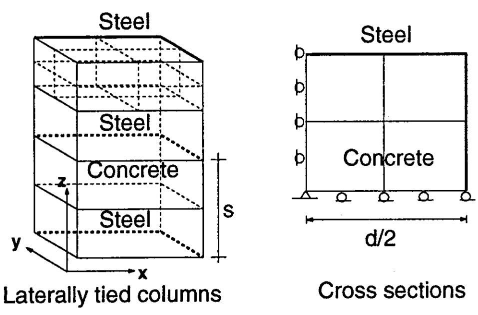

Fig.27 Finite element discretization

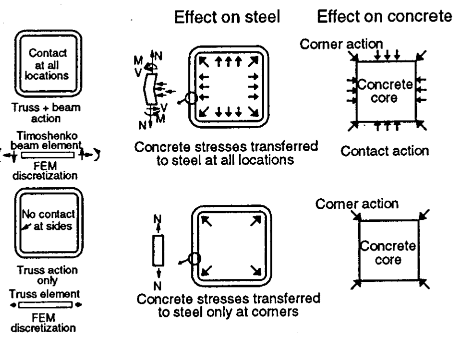

Fig.28 Confinement mechanism of lateral ties

The confinement effectiveness of lateral reinforcement is quantified by the confinement effectiveness index denoted by α[3], which is the ratio of actually induced spatial average confining stress at the peak strength of the confined core to the potential confinement capacity ($\sigma_{v,lim}$) when all lateral steel reaches yield, as described by Eq.(6).

A higher confinement effectiveness is reflected in increased axial compressive capacity of the confined concrete core and related ductility. To verify the micro-mechanical approach at the member level, both confinement effectiveness and capacity enhancement have to be considered.

4.2 Flexural Effect of Lateral Reinforcing Bars

In RC structural analysis, it is generally assumed that reinforcing steel only carries axial stress as a truss or chord member. This hypothesis provides a lateral reinforcement member with finite axial stiffness and infinitely small flexural stiffness so it applies confinement only at the corners of a square concrete core.

The lateral reinforcing bars used in practice however, have a finite flexural stiffness which might contribute to the confinement mechanism. Neglecting this effect might result in underestimating the confinement efficiency of the steel. In implementing 3D micro-mechanical constitutive models of concrete for the evaluation of confinement phenomena, it is necessary to identify the most appropriate model for lateral steel. For this purpose, modeling as truss and beam elements has to be investigated.

To differentiate between the two idealizations, the results of a special experiment which recreates the confinement stress conditions that would be developed in only corner-confined concrete are used. Here, contact between concrete and lateral steel was eliminated by inserting a deformable spacer, except at the corners, resulting in stress transfer only at the four corners of the square core. This condition leads to axial forces only in the ties. A normally confined column with the same confinement parameters and continuous contact between steel and concrete was also used for comparison. The confinement mechanisms in these two experiments are illustrated in **Fig.28**. To simulate the experimental results of axial mean stress-strain and confinement using FEM analysis, steel was modeled as truss and Timoshenko's beam members for the two cases, respectively. Since heavily reinforced columns contain larger diameter bars that inevitably have shear stiffness, Timoshenko's beam theory, which allows shear deformation, is realistic and thought to be appropriate as a lateral tie model.

The observed and computed axial peak strengths of the confined core given in **Fig.29** for the corner acting case are seen to match very closely along the stress-stain paths. In particular, the accuracy of member strength has much to do with the constitutive model for continuum fracturing.

On the other hand, the computed deformability and ductility are dominated by the model for plastic evolution. The mean axial strain at the peak load is seen to be higher in the experiments as compared with analysis using the original plastic evolution law. This may be attributable to the strain rate used in developing the microscopic concrete model (10-100μ/sec), which was higher than that used in experiment (0.1-1μ/sec). **Figure 29** gives analytical results based on factored plastic evolution (β=1.5) as stated in Eq.(10). The computed strength gain computed is not affected, but the ductility prediction is much improved.

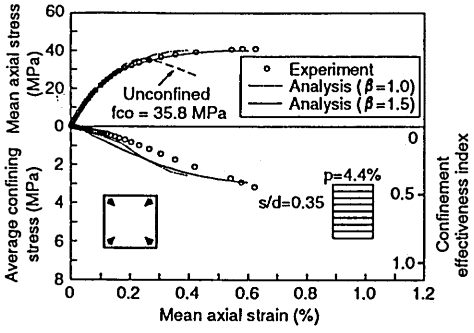

Fig.29 Corner confined column
(Truss element is used in analysis.)

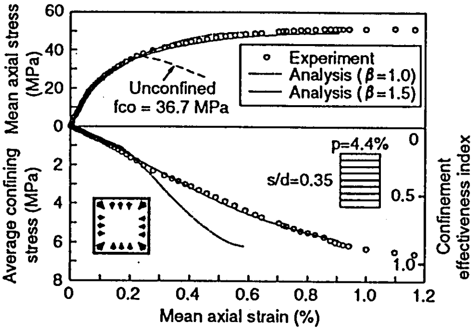

Fig.30 Normally confined column
(Timoshenko's beam element is used in analysis.)

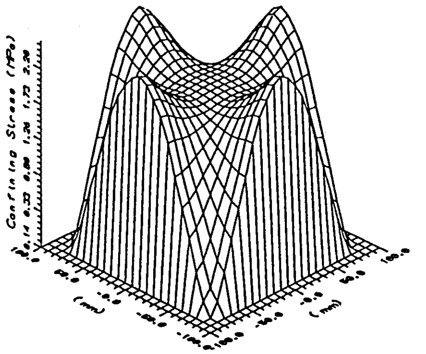

Fig. 31 Confining stress at critical section
(steel idealized as truss elements)

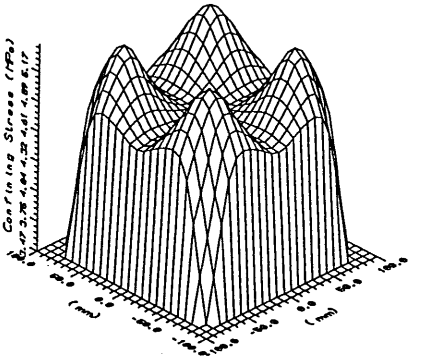

Fig.32 Confining stress at critical section
(steel idealized as beam elements)

These results show that this special experiment is a reasonable physical representation of the truss idealization of steel in the FEM simulation.

Similar results for the companion normal specimen are shown in **Fig.30**. In this case, the experimentally developed peak strength, strain at capacity, and induced average confining stress at the peak are much higher than in the special experiment. This structural enhancement can be directly attributed to the contact or beam effect of lateral ties. A comparison with the FEM analysis data based on beam elements shows that peak strength as well as spatial average confining stress developed at the peak strength are very closely matched by the FEM results.

Strain at peak stress is underestimated when the original plastic evolution law is used, a trend similar to that identified in Fig.30. This observation can be explained again on the grounds of the strain rate used in the experimental development of the microscopic concrete model. In fact, when the same factored plasticity (β=1.5) is applied, overall ductility is also improved.

As a further clarification of the two idealization methods, we compare confinement stress uniformity at the critical section of the core. The critical section governing the peak strength of the core is the midway point between two discretely placed lateral ties. The results of FEM analysis are used to compute the distribution of local lateral confining stress σ_c defined as the in-plane lateral stress invariant given by Eq.(3).

The computed lateral confining stress distribution in the idealized truss case[3)] is shown in the three-dimensional illustration in **Fig.31.** A similar diagram for the case of the idealized beam is depicted in **Fig.32.** At the four corners, the in-plane normal stresses in x- and y-directions are exactly zero because concrete at the corner of the critical section between ties has a free surface on which no external force is applied. Thus, the confining stress defined by Eq.(3) is zero at the four corners. These diagrams show that the confinement stress

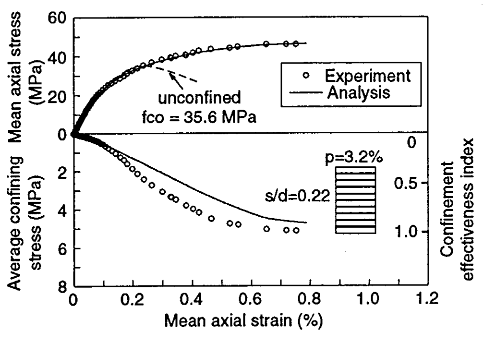

Fig.33 Mean axial stress-strain and confinement (p=3.2%, s/d=0.22)

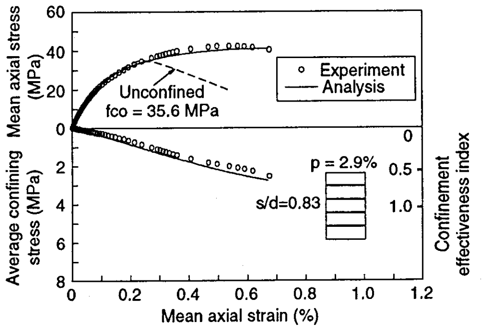

Fig.34 Mean axial stress-strain and confinement (p=2.9%, s/d=0.83)

distribution across the cross section of the core is more uniform in the case of beam element analysis. Furthermore, the absolute values of the confining stresses are be much higher in this case as compared to the truss element analysis. This means that more confinement is applied to the core concrete if the steel is modeled as beam elements than truss elements. These observations further indicate the appropriateness of modeling the confining reinforcement as beam elements.

From these experimental and analytical comparisons, it is clear that for simulation of general confinement phenomena, the lateral steel should be modeled as beam elements rather than the analytically simpler truss elements in the case of the heavily reinforced columns of lateral steel. Even if the lateral reinforcement were light, larger diameter bars with greater bending stiffness are used as a confinement agent in the case of larger spacing. Therefore, it is preferable to use the beam idealization regardless of the amount of lateral ties specified.

4.3 Confinement Effectiveness: Capacity of Core Concrete

The idealized experimental investigation was conducted over a wide range of lateral reinforcement content and spacing. The lateral reinforcement content is quantified in terms of volumetric lateral reinforcement ratio (*p*). The spacing of lateral reinforcement, normalized by the minimum core dimension (*s/d*), is used as the geometry factor of lateral ties. The confined core is assumed to be bound by the centerlines of the peripheral lateral reinforcement.

Since the flexural and shear stiffness of lateral ties is found to dominate confinement, as discussed in the previous chapter, the following FEM analysis is based on steel idealized as beam elements. A comparison of FEM simulation results pertaining to confinement level and strength of the confined core at peak strength with the experimental results is given in **Table 6**. Here, the maximum available confining stress, denoted by $\sigma_{v,\lim}$ in Eq.(6), is reached if all lateral steel attains the yield condition at the core peak given by $\frac{1}{2}pf_y$.

(1) Axial Mean Stress and Confinement Stress

The relation of most interest in regard to the macro behavior of confined concrete columns is the mean axial stress-strain variation. The objective of the microscopic approach is to correctly predict this non-linearity up to the peak strength of concrete. Through this approach, a curve is cumulatively generated based on elasticity, plasticity, and continuum damage.

To understand the trends indicated by the analytical method as compared with experimental results, three pairs of specimens are considered in the following discussion. Since the yield strength of lateral steel for this study is kept nearly constant, the reinforcement ratio is a direct indicator of potential confinement.

The mean axial stress-strain relations, both experimental and computed, for nearly the same ($p \cong 3\%$) lateral reinforcement ratio with different spacing ratios are studied first. This medium reinforcement ratio was selected as a demonstration of the standard conditions used in the experimental program. Experimental and analytical results are compared in **Fig.33** for a closely spaced column and in **Fig.34** for more widely spaced

Table 6 FEM analysis results at peak strength for confined columns in the experimental program

Designation and Comments	Spacing ratio (s/d)	Average confining stress (σ_v) (MPa)			Strength of core concrete (MPa)		
					Unconfined (f_{co})	Confined (f_{cc})	
		Max. available	Exp.	FEM		Exp.	FEM
C16-075 high r/f	0.41	9.49	7.64	6.58	36.9	59.5	50.7
D19-104 high r/f	0.58	9.24	7.20	5.43	35.6	53.5	46.8
O19x2-232 high r/f	1.20	8.49	1.72	1.60	35.2	39.0	38.2
A09-042 medium r/f	0.22	5.40	5.06	4.71	35.6	46.3	46.4
H13-094 medium r/f	0.51	4.99	3.67	3.69	35.6	43.9	43.3
I16-150 medium r/f	0.83	4.56	2.11	2.77	35.6	42.6	41.1
J19-225 medium r/f	1.26	4.38	1.07	1.76	35.6	39.9	38.8
M09-090 low r/f	0.48	2.52	1.80	2.12	35.2	40.3	40.0
N13-192 low r/f	1.04	2.45	0.64	1.41	35.2	37.7	38.0
P09-043 small core	0.31	7.13	6.38	6.03	38.0	53.0	51.2
S25-119 big core	0.32	6.61	5.63	5.54	37.3	51.3	49.5
T13-065 size effect flex. Effect	0.35	7.22	6.56	5.84	36.7	51.8	49.0
U13-065-C corner action	0.35	7.22	3.15	2.92	35.8	41.1	39.9
V16-075-LS high r/f low f_{co}	0.41	9.12	7.18	5.22	27.5	46.4	38.6

Note) Compression is specified as positive in this table.

one. The confinement effectiveness index is also placed on the same axis as the spatial average confining stress to provide an indication of the level of confinement.

It is seen that for both columns the FEM prediction of peak strength matches fairly well. For the column with the lower spacing ratio, the computed mean axial stress-strain path matches the experimental observations quite well. The induced average confining stress path is predicted fairly well by the analysis at the beginning of loading and around the peak strength of the core. In the case of higher spacing, the mean axial stress-strain path as well as the confining stress path is very closely predicted. The peak strength of the core concrete and the strain at peak strength are also predicted very well.

The computed stress-strain relation is compared with the experimentally observed one for low (p=1.5%) and medium (p=2.8%) reinforcement ratio with spacing ratios above unity. The spacing ratios are s/d=1.04 and s/d=1.26, respectively. The physical meaning of this spacing condition is that the ties are arranged with a

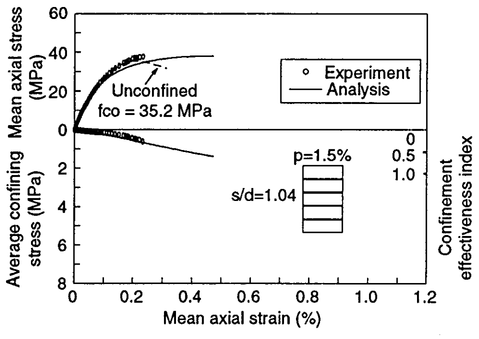

Fig.35 Mean axial stress-strain and confinement (p=1.5%, s/d=1.04)

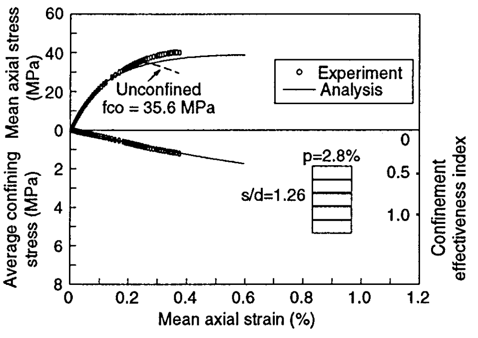

Fig.36 Mean axial stress-strain and confinement (p=2.8%, s/d=1.26)

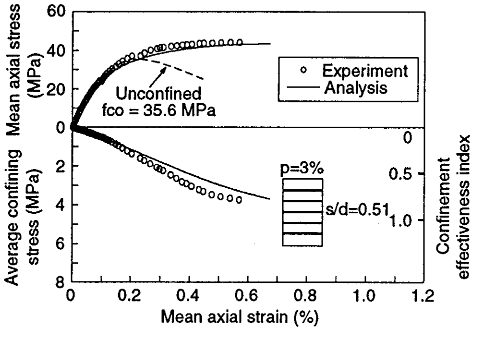

Fig.37 Mean axial stress-strain and confinement (p=3.0%, s/d=0.51)

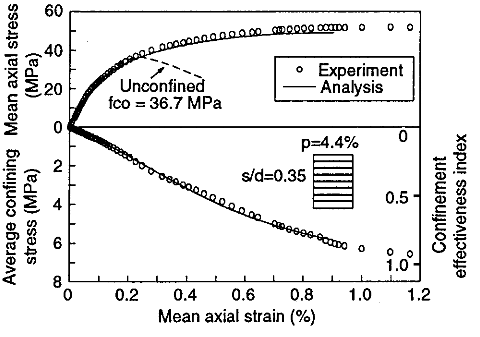

Fig.38 Mean axial stress-strain and confinement (p=4.4%, s/d=0.35)

spacing that exceeds the core size. The mean axial stress-strain as well as the induced average confining stress versus mean axial strain of the core are given in **Fig.35** and **Fig.36**, respectively. At the lower reinforcement ratio shown in **Fig.35**, it can be seen that the strength matches quite well. However, the experimental mean axial strain at peak strength is lower than the analytical prediction by about 50%. This discrepancy might be attributable to the instability which occurs in the core concrete close to the peak, since the spacing is quite large. The experimental induced average confining stress is also about 50% lower than the predictions at the peak strength of the core. Nevertheless, the absolute values of these average confining stress are small. In the medium reinforcement case presented in **Fig.36**, the peak strength prediction is satisfactory. Still, there is overprediction of the strain at peak strength, as in **Fig.35**. Further, it is clear that the change in induced confinement is predicted well until the peak of experimental data.. Confinement at the peak strength of the core is overpredicted by the analysis.

A typical set of curves for practically applicable lower spacing ratio are considered as the third pair. The mean axial stress-strain curve and induced average confining stress against mean axial strain curves are plotted in **Fig.37** for a volumetric reinforcement ratio of 3.0% with a spacing ratio of 0.51. The peak strength and axial stress-strain paths are quite well matched in this case. The analytical induced confining stress is also seen to follow the experimental curve quite closely. A deviation is observed near the peak strength. For the higher reinforcement ratio (p=4.4%), and with spacing ratio of 0.35, the curves are shown in **Fig.38**. Both axial peak strength and the axial mean stress-strain curves for the analytical and experimental results are closely matched. However, there is some underprediction of the experimental value for strain at the peak strength of the core. The induced confining stress is seen to match very closely to the experimental value at the peak strength of the core.

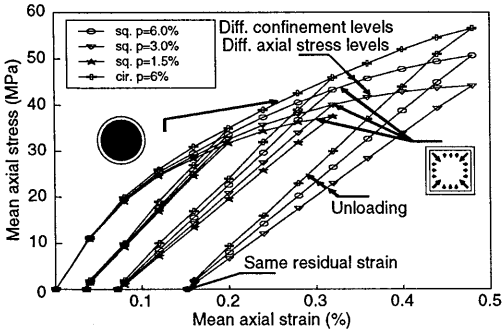

Fig.39 Analytical response of confined cores under cyclic loading

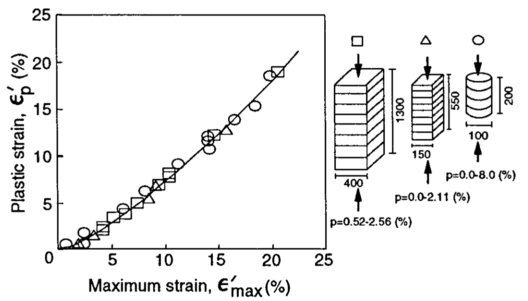

Fig.40 Experimentally obtained residual strains for different confinement levels and sections[21)]

These six comparisons indicate that the peak strength is quite well predicted while the strain at the core peak strength deviates. This could be attributable to the different strain rates used in developing the material relations for the micro model as compared with the experiments, as mentioned before. It can be noted in these curves that, for lower spacing ratios (i.e. closely spaced ties), the analytical predictions of peak strength and confining stress at peak strength generally match quite well. For higher spacing conditions, the analytical method predicted the peak strengths quite closely.

However, the analysis has a general tendency to slightly overpredict the confining stress level at the peak strength of the core for large spacings. In the case of a small reinforcement ratio with a closer arrangement of ties, both strength gain and confinement effectiveness were fairly well predicted. This behavior will be discussed again for other combinations of lateral reinforcement ratio and spacing in a later section.

(2) Cyclic loading

As a further discussion of the characteristics of the approach based on the microscopic constitutive law, unloading and residual deformations are now considered. **Figure 39** shows axial stress-strain relations for three cases of square concrete cores and one circular core with different confinement levels. These four levels were generated using same-sized lateral ties placed at different spacings, resulting in varying lateral reinforcement ratios. In this analysis, beam idealization was adopted for the square cores, while truss idealization was used for the circular core, since there is no bending moment owing to the point symmetry around the center of the section. In the simulations, unloading was commenced at three discrete levels of axial mean strain.

It is noteworthy that the residual axial strains are not influenced by the different axial stress levels at the start of unloading. Experimental verification for this phenomenon is available in reference 21), where laterally confined square and circular concrete columns were subjected to cyclic axial compressive loading. At the conclusion of each cycle, the residual axial strain was plotted against the maximum axial strain to which the column had been subjected. These results are shown in **Fig.40**. Clearly the relation between residual axial strain and maximum axial strain is not influenced by the confining arrangement or shape, which represent different levels of confinement. It can be said with reference to this figure that the residual plastic deformation under axial loading is not affected by the level of confinement as formulated in Eq.(10). These observations at the member level verifies the constitutive law, which indicates that the relation between plastic deviatoric strain and elastic deviatoric strain is not influenced by the confinement level as shown in **Fig.25**.

Another advantage of confinement is identified by this discussion; it allows confined concrete to attain higher axial stress levels without generating excess residual plastic deformations. The practical significance of this is realized when confined members are subjected to repeated overloading; the result is lower permanent deformations, indicating better serviceability.

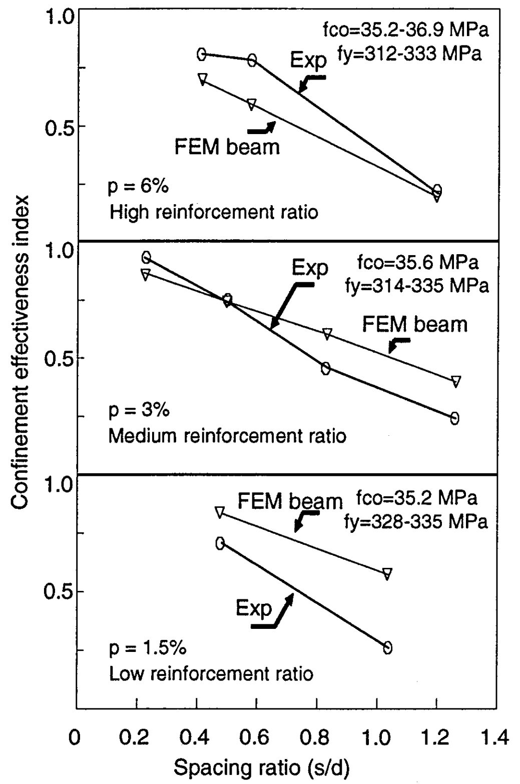

Fig.41 Confinement effectiveness index against tie spacing and reinforcement ratio

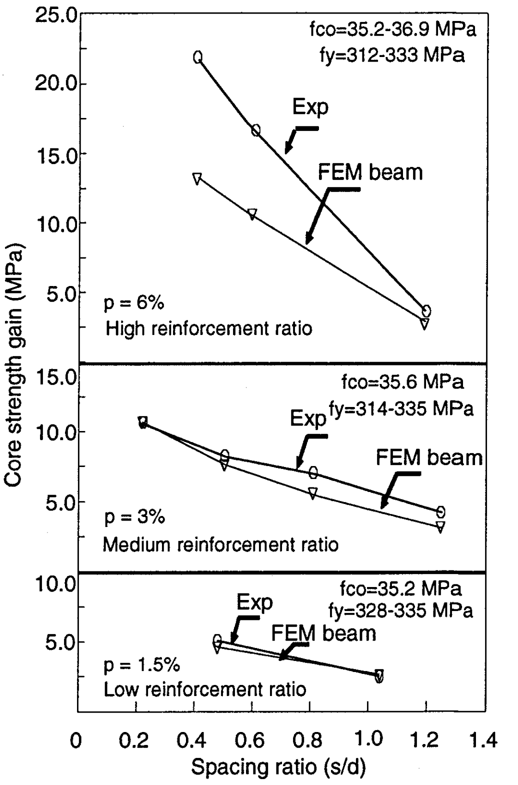

Fig.42 Core strength gain against tie spacing and reinforcement ratio

(3) Spacing and Amount of Lateral Reinforcement

The spacing and amount of lateral reinforcement, which are the most influential factors in the effect of confinement at the peak strength of the confined concrete core, are now addressed as a further discussion of the appropriateness of the micro-mechanical approach. For this purpose, three ranges of reinforcement content are selected. The reinforcement content, given in terms of volumetric reinforcement ratio, is a direct indicator of the potential confinement, since the steel yield strength was almost invariant.

The values of confinement effectiveness index obtained from experiments as well as FEM analysis are compared for different spacings under the three lateral reinforcement levels in **Fig.41**. The FEM analysis results with lateral steel idealized as beam elements are seen to be close to the experimentally observed values for closely spaced conditions (s/d<0.6) in all three ranges of reinforcement content. For higher spacing, a general tendency for FEM to overpredict is observed.

As further verification, **Fig.42** shows the core strength gains due to confinement at the peak strength by experiment and analysis, for the same ranges as discussed above. It is observed that for lower to medium reinforcement contents (p=1.5% - p=3%) the strength gains are predicted quite well for all spacings. At the higher reinforcement content (p=6%), a general tendency to underpredict the strength gain is exhibited by the analytical method.

In consideration of both confinement effectiveness index and strength gain at the peak strength of the confined concrete core, it is clear that the FEM analytical method successfully in simulates the behavior when the lateral reinforcement is closely placed (s/d < 0.6) and the content is less than 4.4%. A reinforcement content of 4.4% at lower spacing was also seen to produce good results for both confinement effectiveness index and strength gain, as indicated in **Fig.42**. This verified range is of much practical importance since it represents normally used lateral reinforcement configurations. Higher spacings are not suitable due to the low confinement effectiveness, while higher lateral reinforcement ratios are not practicable in ordinary confined columns with longitudinal reinforcement.

5. CONCLUSIONS

Experimental observations carried out against a theoretical conceptual background have offered a valuable insight into the phenomenon of passive lateral confinement by steel ties in square columns under axial compressive loading. Through this study, mechanically defined spatial average confining stress was measured for the first time for square lateral reinforcement. Confinement effectiveness index with a mechanical basis was introduced as the ratio of the above average confining stress to the potential confinement capacity of the lateral reinforcement.

Lateral steel does not always reach yield at the peak strength of a square confined core as assumed in many previous studies. This was experimentally demonstrated through spatial strain measurements in lateral ties which were converted to a stress distribution. Consequently, the actually developed confinement does not reach the maximum potential confinement capacity, indicating that there is no direct relation between the potential confinement and the enhancement in strength of a confined core.

The actually developed spatial average confining stress was found to be a basic governing quantity for confinement effectiveness and strength enhancement due to confinement. Through the experimental program, the amount of the lateral reinforcement -- in terms of volumetric lateral reinforcement ratio and tie spacing expressed as the ratio of spacing to core dimensions -- was found to be the most influential on the induced spatial average confining stress. Secondly, the flexural contribution of lateral tie arms – which depends on the diameter and span of each arm and its contact action -- was found to have a significant beneficial effect on the confinement action. Therefore, this effect should not be neglected in analytical formulations of confinement effectiveness.

The strength gain of a confined core was found to be influenced by the developed average confining stress and the spacing of the ties, which governs the lateral confining stress uniformity. Since the developed average confining stress is also dependent on the tie spacing, it was found to have a double effect on strength enhancement due to confinement.

The core size was found to have no appreciable effect on the confinement effectiveness of lateral ties in the range examined (core size range 139 mm -373 mm).

In order to verify a non-linear three-dimensional elasto-plastic and continuum fracture model at the laterally reinforced concrete member level through FEM analysis, idealized experimental results on axially loaded confined columns were used.

Based on the results of a special experiment in which confinement was applied only at the corners (with contact between tie arms and concrete eliminated), the truss idealization of the lateral steel in the FEM method was verified. Through this verification it was shown that steel reinforcement should be modeled as beam members capable of resisting flexure and shear in the simulation of actual confined concrete cores. This is in contrast to the common analytical assumption that reinforcement should be modeled as truss members. Comparisons were carried out between typical experimental results and analytical results based on a beam idealization of reinforcing steel. Mean axial stress-strain relations until the peak strength of the confined concrete were compared in conjunction with spatial average confining stress. Special attention was paid to the peak strength level, due to its particular significance.

FEM simulations of axial cyclic loading of confined concrete indicated that the confinement level does not influence the residual strain when the maximum induced strain experienced in the loading paths is the same. This was verified by experimental results on cyclically loaded concrete cores.

From these comparisons, it is concluded that the behavioral trends observed in experiments were closely simulated by the analytical method throughout the lateral reinforcement detailing ranges considered. On a quantitative basis, the three-dimensional FEM method was shown to be effective in simulating confinement effectiveness and strength enhancement when smaller spacings (s/d <0.6) are adopted with medium to low reinforcement ratios (p<4.4%). These ranges are significant since the verified applicability of the analytical method represents the practical application domain.

In a case where much heavy reinforcement is used (p>4.4%), computations based on the constitutive model result in underestimation of the strength of the confined cores. This underestimation is thought to be rooted in the insufficient accuracy of the fracture evolution model in the constitutive law under higher confinement conditions, as pointed out in reference 5). For further improvement of the constitutive model, the plasticity and fracturing evolution rules under much higher confinement conditions should be further investigated.

ACKNOWLEDGMENT: The authors express their gratitude to Professor Hajime Okamura of the University of Tokyo for his guidance. This study was financially supported by Grant-in-Aid for scientific research No.05452226 and No.04555114 from The Ministry of Education of The Japanese Government.

REFERENCES

1) Sheikh, S. A., and Uzumeri, S. M.: Strength and Ductility of Tied Concrete Columns, *Proceedings*, ASCE, Vol. 106, pp. 1079-1102, 1980

2) Carreira, D. J., and Chu, K. H.: Stress-Strain Relationship for Plain Concrete in Compression, *American Concrete Institute Journal*, Vol. 82, pp. 797-804, 1985

3) Irawan, P., and Maekawa, K.: Three-Dimensional Analysis of Strength and Deformation of Confined Concrete Columns, *Concrete Library*, JSCE, No. 24, pp.47-69, 1993

4) Okamura, H., and Maekawa, K.: *Nonlinear Analysis and Constitutive Models of Reinforced Concrete*, Gihodo-Shuppan, Tokyo, 1991

5) Maekawa, K., Takemura, J., Irawan, P., and Irie, M.: Triaxial Elasto-Plastic and Continuum Fracture Model for Concrete, *Concrete Library*, JSCE, No. 22, pp. 131-161, 1993

6) Okamura, H., Maekawa, K., and Ozawa, K.: *High Performance Concrete*, Gihodo-Syuppan, Tokyo, 1993. (in Japanese)

7) Gangadharam, D., and Nagi Reddy, K.: Effect of Cover Upon the Stress-Strain Properties of Concrete Confined in Steel Binders, *Magazine of Concrete Research*, Vol. 32, pp. 147-155, 1980

8) Karsan, I. D., and Jirsa, J. O.: Behavior of Concrete Under Compressive Loadings, *Journal of the Structural Division*, ASCE, Vol. 95, pp.2543-2563, 1969

9) Sargin, M.: Stress-Strain Relationships for Concrete and Analysis of Structural Concrete Sections, *Study No. 4*, Solid Mechanics Division, University of Waterloo, Waterloo, Ontario, Canada, 1971

10) Scott, B. D., Park, R., and Priestley, M. J. N.: Stress-Strain Behavior of Concrete Confined by Overlapping Hoops at Low and High Strain Rates, *ACI Journal Proceedings*, Vol. 79, pp. 13-27, 1982

11) Somes, N. F.: Compression Tests on Hoop Reinforced Concrete, *Proceedings*, ASCE, Vol. 96, pp. 1495-1509, 1970

12) Brudette, E. G., and Hilsdorf, H. K.: Behavior of Laterally Reinforced Concrete Columns, *Journal of the Structural Division*, ASCE, Vol. 97, pp. 587-602, 1971

13) Bangash, M.Y.H.: *Concrete and Concrete Structures: Numerical Modeling and Applications*, Elsevier Applied Science, London, 1989

14) Task Committee on Finite Element Analysis of Reinforced Concrete Structures of the Structural Division Committee on Concrete and Masonry Structures, *Finite Element Analysis of Reinforced Concrete,* ASCE, New York, 1982

15) Maekawa, K., and Okamura, H.: The Deformational Behavior and Constitutive Equations for Concrete Using Elasto-plastic and Fracture Model, *Journal of the Faculty of Engineering*, The University of Tokyo (B), 37(2), pp. 253-328, 1983

16) Chen, W.F., and Saleeb, A.F.: *Constitutive Equations for Engineering Materials, Vol. 1 : Elasticity and Modeling*, John Wiley & Sons, New York, 1982

17) Ahmad, S.H., and Shah, S.P.: Behavior of Hoop Confined Concrete under High Strain Rates, *ACI Journal*, Vol. 82, pp. 634-647, 1985

18) Chen, W.F.: *Plasticity in Reinforced Concrete*, McGraw Hill Book Co., New York, 1982

19) Dilger, W.H., Koch, R., and Kowalczyk, R.: Ductility of Plain and Confined Concrete under Different Strain Rates, *ACI Journal*, Vol. 81, pp. 73-82, 1984

20) Zienkiewicz, O. C.: *The Finite Element Method*, McGraw-Hill, 1977

21) Maekawa, K., Song, C., and Irie, M.: Unified Concept for Compressive Characteristics of Concrete -- From 3D Confinement to Pre-cracking, *JCI Colloquium*, Analytical Studies on Shear Design of Reinforced Concrete Structures, pp. 31-38, 1989